Monthly Notices
of the
ROYAL ASTRONOMICAL SOCIETY

Mon. Not. R. Astron. Soc. **419,** 342–357 (2012) doi:10.1111/j.1365-2966.2011.19697.x

SX Phoenicis period–luminosity relations and the blue straggler connection

Roger E. Cohen⋆ and Ata Sarajedini

Department of Astronomy, University of Florida, 211 Bryant Space Sciences Center, Gainesville, FL 32611, USA

Accepted 2011 August 24. Received 2011 August 23; in original form 2011 July 7

ABSTRACT

This study is aimed at investigating the period–luminosity relation of SX Phoenicis (SX Phe) pulsators in Galactic globular clusters (GGCs) and Local Group dwarf galaxies. We verify isochrone-fitting distances of 46 GGCs by fitting their main sequences to a carefully chosen set of nearby, unevolved subdwarfs. We find that the difference between cluster distances obtained via isochrone fitting by Dotter et al. and those resulting from our subdwarf fits has a mean of 0.094 mag and a standard deviation of 0.098 mag. The cluster distances from Dotter et al. are used to calibrate an SX Phe period–luminosity relation based on radial double mode pulsators. The resulting empirical period–luminosity relation, which is insensitive to the inclusion of colour and/or metallicity terms, generally agrees well with previous empirical relations as well as theoretical predictions based on single-star pulsational and evolutionary models. However, there is a subset of 'subluminous' variables identified most notably in Fornax, Carina, NGC 2419 and Omega Centauri. We explore the possibility that, at least in GGCs, they represent blue stragglers which have enhanced helium content that was either inherited from second-generation progenitors or gained as a result of the blue straggler formation process.

Key words: stars: variables: δ Scuti – globular clusters: general – distance scale.

1 INTRODUCTION

The class of variables known as SX Phe stars are low-luminosity instability strip pulsators which are generally considered the Population II analogues of δ Scuti stars. At least as early as Frolov (1974), it became apparent that these stars are systematically more metal poor and less luminous than their δ Scuti counterparts. Nemec & Mateo (1990) presented an early compilation of SX Phe in Galactic globular clusters (GGCs); they also imply that they may be useful as distance indicators and show that they occupy a narrow subregion of the instability strip in colour. Nemec, Linnell Nemec & Lutz (1993) derived a period–luminosity relation which included a metallicity term; as the size of the observed sample of SX Phe grew, various empirical period–luminosity relations were proposed based on individual clusters (e.g. Jeon et al. 2003, 2004a) as well as ensembles of SX Phe and δ Scuti stars (e.g. McNamara et al. 2004; Poretti et al. 2008, hereafter P08). Accordingly, grids of linear non-adiabatic SX Phe pulsational models have been computed by Santolamazza et al. 2001 (hereafter S01), Templeton, Basu & Demarque (2002), Petersen & Freyhammer (2002, hereafter PF02) and Olech et al. (2005) in addition to existing metal-rich δ Scuti models (e.g. Petersen & Christensen-Dalsgaard 1999, hereafter PCD99; Bono et al. 1997 and references therein).

The astrophysics of SX Phe variables is of particular interest because in GGCs, the region of the instability strip which they occupy in a colour–magnitude diagram is coincident with the blue straggler region (e.g. Jeon et al. 2004a). This is an important evolutionary distinction between SX Phe and δ Scuti pulsators since δ Scuti are often found on the main sequence (e.g. Rodríguez & Breger 2001), although δ Scuti in both pre- and post-main-sequence phases of stellar evolution have been identified as well (e.g. Lenz et al. 2010; Marconi et al. 2010).

Information on the interiors of SX Phe stars ascertained through an analysis of their pulsation frequencies has been proposed as a viable avenue to gain further clues to the as-yet-unsolved issues of blue straggler star (BSS) formation and evolution (e.g. Olech et al. 2005). A handful of individual cases of interest have been identified in GGCs, including V41 in M55 (Pych et al. 2001) and NV313 in ω Cen (Olech et al. 2005). However, aside from the lack of a large global helium enhancement for a large sample of SX Phe stars (Olech et al. 2005), it seems that observationally, SX Phe have not yet provided strong constraints regarding the complicated issue of BSS formation.

The number of known short-period instability strip pulsators has more than doubled in recent years. This is true not only of GGCs, but also for extragalactic populations in the Local Group. Recent photometric variability surveys of Local Group galaxies have revealed short-period instability strip pulsators in Fornax (P08), its cluster Fornax 5 (Greco et al. 2009), Leo IV (Moretti et al. 2009), IC 1613 (Bernard et al. 2010), and the Large Magellanic Cloud

⋆E-mail: cohenr@astro.ufl.edu

(LMC) cluster NGC 2155 (Otulakowska et al. 2011), in addition to the known SX Phe population of Carina (Mateo, Hurley-Keller & Nemec 1998; Poretti 1999).[1] Furthermore, systematic large-scale surveys continue to increase the size and quality of the short period variable sample in the Magellanic Clouds (e.g. Poleski et al. 2010). Given this large recent increase in the amount of data available for both GGCs and extragalactic populations, it is important to reanalyse the sample of known SX Phe and δ Scuti, with an eye towards SX Phe in GGCs because of their unusual evolutionary histories.

Rather than investigating individual cases in detail, we use the known SX Phe population as an ensemble to explore the connection between SX Phe and blue stragglers. Specifically, by using a newly expanded data base of SX Phe in GGCs, supplemented with those discovered in Local Group dwarf galaxies and their clusters, we can ask whether blue stragglers obey a separate period–luminosity relation from that predicted by 'normal' single star pulsational and evolutionary models, yielding information about blue straggler formation histories. The concept that blue straggler evolution depends on formation history (Iben 1986) may manifest itself observationally if blue stragglers formed from collisions are well mixed (Lombardi, Rasio & Shapiro 1995). In this scenario, blue stragglers formed from the coalescence of a binary system would show anomalous surface abundances due to the accretion of material from deep inside the donor star (Sarna & De Greve 1996). The ability to use abundances of blue stragglers to differentiate between their formation mechanisms, predicted by Bailyn (1992), recently gained strong observational support in the spectroscopic work of Ferraro et al. (2006). They identified two subpopulations of blue stragglers in 47 Tuc, one of which displays normal subgiant-like abundances, and the other of which shows anomalous carbon and oxygen abundances and contains two W Ursae Majoris binaries suspected of ongoing mass transfer. There seems to be a general consensus that the vast majority of blue stragglers are formed from binaries, although dynamical encounters likely play an important role in this process as well (e.g. Knigge, Leigh & Sills 2009; Leigh, Sills & Knigge 2011). However, the effect of blue straggler formation and evolution on their pulsational properties is an open issue which we seek to address.

Since we are focusing on pulsating variables in this paper, it is also appropriate for us to address the issue of the period–luminosity relations for these stars. These are often calibrated using nearby pulsators with well-determined parallaxes, circumventing the effects of reddening via reddening-independent Wesenheit indices (van den Bergh 1968; Madore 1982). While this approach has the advantage that multiple types of pulsators can be used simultaneously to gain leverage on distance determinations (e.g. Majaess et al. 2011), it also currently suffers from two specific disadvantages. First, there are a small number of calibrators which have sufficiently precise parallaxes (especially in the case of SX Phe, of which the namesake of the class is the sole example). Secondly, there is the dependence of the Wesenheit index on colour rather than just magnitude, requiring uniform photometry in two bandpasses for all of the calibrators. We wish to explore an alternative approach using the now sizeable population of SX Phe in GGCs as an ensemble to calibrate a period–M_V relation. Because the success of our approach rests largely on the accuracy and homogeneity of GGC distances, we will redetermine distances to GGCs in our sample by fitting their main sequences to field subdwarfs with well-measured parallaxes. While individual cluster distance moduli obtained via subdwarf fitting typically have uncertainties of $\sim$0.1 mag even in the best cases (e.g. Richer et al. 1997; Testa et al. 2004), the use of 46 individual clusters allows for statistical tests of any discrepancies between our distances and those in the literature.

The remainder of this paper is organized as follows. In Section 2, we describe the selection of subdwarfs to be used for the main-sequence fitting, the relevant uncertainties, and a comparison of the resultant GGC distances to the distances reported by Dotter et al. (2010, hereafter D10). In Section 3, we use distances from D10 to place GGC and Local Group SX Phe on dereddened colour–magnitude diagrams and calibrate SX Phe period–luminosity relations to analyse the pulsational and photometric properties of the SX Phe in our updated catalogue. Also, we compare our period–luminosity relations with previous empirical and theoretical relations using extragalactic SX Phe and δ Scuti as test beds. In Section 4, we summarize our results along with remaining unsolved questions, and describe avenues for further investigation from both observational and theoretical standpoints.

2 GLOBULAR CLUSTER DISTANCES VIA SUBDWARF FITTING

Our strategy is to capitalize on the homogeneity of the GGC metallicity scale of Carretta et al. (2009, hereafter C09), including subdwarf abundances determined by Gratton et al. (2003a, and references therein). A large compilation of precise subdwarf photometry was recently presented by Casagrande et al. (2010, hereafter CRMBA). By showing that the metallicities of CRMBA and those of C09 and Gratton et al. (2003a) are in agreement, we can simultaneously exploit the consistency of the C09 abundance scale and the CRMBA subdwarf photometry.

2.1 Cluster fiducial sequences

Our source of GGC photometry is the Advanced Camera for Surveys (ACS) Galactic Globular Cluster Treasury Project (Sarajedini et al. 2007). This survey consists of deep ($\sim$7 mag below the main-sequence turn-off), precise (S/N $\sim$ 10 for 0.2 $M_\odot$) photometry of 65 GGCs in two filters ($F606W$ and $F814W$) obtained with the ACS Wide Field Camera (WFC) onboard *Hubble Space Telescope* (*HST*). Using these data, fiducial main sequences were constructed by calculating the median colour value in 0.2 mag bins. Clusters with broadened or multiple main sequences (e.g. Piotto et al. 2005, 2007; Anderson et al. 2009; Milone et al. 2010) were excluded from this analysis, leaving a total of 46 clusters for which we can compare D10 isochrone-fitting distances and our subdwarf-based distances.

The ACS photometry for each cluster was dereddened using the reddening values given by D10 and the extinction coefficients and reddening law from Sirianni et al. (2005). It is important to note that Sarajedini et al. (2007) find that the reddening values we have adopted are in good agreement with the Schlegel, Finkbeiner & Davis (1998) reddening maps. Hence, we assign the cluster reddening values an uncertainty of 0.01 when calculating the total uncertainties in our subdwarf-based cluster distance moduli.

2.2 The subdwarf sample

Our candidate subdwarfs for main-sequence fitting were drawn from those presented by CRMBA with $(V - I)$ photometry, $M_V > 5$ and $\sigma_\pi/\pi \leq 0.10$ based on the new *Hipparcos* reduction

[1] Musella et al. 2009 discovered a variable blue straggler in Coma Berenices as well, but its nature remains uncertain and on the basis of its light-curve shape, they suspect it of being a binary rather than a pulsator.

(van Leeuwen 2007). We transform the subdwarf $(V - I)$ photometry from CRMBA to the ACS WFC filter system using equations from Sirianni et al. (2005). The reason for this approach, as opposed to transforming the GGC photometry to the ground-based system, is that the subdwarfs, unlike the GGCs, are all nearby and consequently have negligible [$E(B - V) \leq 0.002$] reddening values. The proximity of the subdwarfs, in addition to minimizing any uncertainties or systematic effects of reddening on the transformation between the filter systems, also minimizes the contribution of reddening uncertainties to the total uncertainty of the subdwarf colours. Of our candidate subdwarfs from CRMBA, 13 were also studied by Gratton et al. (2003a, and references therein). Any stars which Gratton et al. (2003a) list as known or suspected binaries were rejected, and in addition we discarded HD 144579, which Raghavan et al. (2010) suspect to be a binary (eight more of our final list of 27 subdwarfs were also included in their survey and no evidence for companions was found). The binary nature of HD 144579 is supported by the discrepancy of this star from a $(B - V) - (V - I)$ relation fit to the remainder of the subdwarfs which met the aforementioned selection criteria.

We use the subdwarf and GGC abundances of C09 and Gratton et al. (2003a) for two reasons. First, [Fe/H] and [α/Fe] values have been systematically measured for a large number of GGCs (C09; Carretta et al. 2010). Secondly, these abundances were derived in a consistent manner for many nearby subdwarfs (Gratton et al. 1997; Carretta et al. 2000; Gratton et al. 2003a). Consequently, we can avoid uncertainties in the main-sequence fitting process caused by the use of different metallicity scales. Furthermore, potential differences between cluster abundances determined using giants and those determined using turn-off and subgiant stars, which are much closer in luminosity to the main-sequence stars used for the fits, are essentially negligible (Gratton et al. 2003b). In addition, to minimize the effect of varying α-enhancement among and between cluster stars and subdwarfs, we choose to evaluate both the subdwarf and cluster metallicities using the global metallicity [M/H] = [Fe/H] + $\log(0.638f + 0.362)$ where $\log f = [\alpha/\mathrm{Fe}]$ following Salaris, Chieffi & Straniero (1993). We assumed a value of [α/Fe] = 0.4 for clusters for which [α/Fe] values are not given (Carretta et al. 2010, see their fig. 5). While the abundances given by CRMBA were not obtained in an identical manner as those of C09 and Gratton et al. (2003a, and references therein), we can use the 13 stars in common between CRMBA and the Gratton et al. (2003a) sample to check for any differences in their respective abundance determinations. Fig. 1 shows the results for [Fe/H], [α/Fe] and the [M/H] values. We find that the mean difference in [M/H] values for all stars in common between both studies is 0.057 ± 0.042 dex. When we restrict our analysis to only bona fide single, unevolved ($M_V > 5$) subdwarfs, this difference is reduced to -0.012 ± 0.044 dex, which is statistically equivalent to zero. Although these 13 subdwarfs admittedly cover a smaller metallicity range than our target clusters ($-1.5 \lesssim$ [M/H] $\lesssim -0.7$ for the subdwarfs, $-2.1 \lesssim$ [M/H] $\lesssim 0$ for the target clusters), a difference of $\sim$0.06 dex in subdwarf [M/H] values would affect our final results at the level of $<$0.01 mag in the mean. Hence, we use the Gratton et al. (2003a, and references therein) abundances when available, and otherwise we use the abundances from CRMBA and Casagrande, Portinari & Flynn (2006). The final sample of subdwarfs, along with their parallaxes and errors from the new *Hipparcos* reduction (van Leeuwen 2007) and the adopted photometric properties and abundances are listed in Table 1. Examples of our subdwarf fits, plotted in the absolute M_{814} plane to illustrate the absolute magnitudes of the subdwarfs, are shown in Fig. 2.

Table 1. The subdwarf sample.

BD/HD	HIP	π (mas)	σ_π/π	V (mag)	$(V - I)$ (mag)	σ_{V-I} (mag)	[Fe/H] (dex)	[α/Fe] (dex)	$\sigma_{[\mathrm{Fe/H}]}$ (dex)
CD-35 0360	5004	15.49	0.10	10.266	0.877	0.015	−0.90	0.39	0.11
HD 8638	6607	25.06	0.04	8.300	0.750	0.015	−0.50	0.12	0.15
HD 10853	8275	41.63	0.03	8.910	1.162	0.015	−0.74	0.21	0.15
HD 11130	8543	39.04	0.02	8.070	0.833	0.015	−0.57	0.15	0.15
BD-01 306	10449	15.87	0.08	9.084	0.696	0.015	−0.96	0.36	0.15
HD 19445	14594	24.92	0.04	8.026	0.632	0.008	−1.91	0.40	0.07
HD 25329	18915	54.68	0.02	8.519	0.973	0.015	−1.80	0.49	0.04
HD 25673	19007	21.09	0.06	9.532	0.910	0.015	−0.53	0.15	0.15
HD 31128	22632	15.00	0.08	9.135	0.634	0.015	−1.86	0.41	0.10
HD 34328	24316	14.72	0.06	9.416	0.643	0.008	−1.44	0.37	0.07
HD 263175	32423	38.11	0.03	8.810	1.060	0.015	−0.59	0.16	0.15
HD 59374	36491	20.20	0.06	8.485	0.650	0.015	−0.88	0.29	0.15
BD+51 1696	57450	12.85	0.10	9.916	0.715	0.015	−1.48	0.33	0.15
HD 108564	60853	36.78	0.03	9.450	1.132	0.015	−1.18	0.40	0.15
HD 119173	66815	18.43	0.06	8.828	0.652	0.015	−0.62	0.15	0.15
HD 120559	67655	39.42	0.02	7.971	0.755	0.015	−0.94	0.33	0.04
HD 126681	70681	21.04	0.05	9.296	0.727	0.015	−1.14	0.32	0.04
HD 132142	73005	42.76	0.01	7.770	0.866	0.015	−0.54	0.24	0.15
HD 134440	74234	35.14	0.04	9.420	0.975	0.015	−1.45	0.19	0.04
HD 134439	74235	34.65	0.04	9.118	0.898	0.008	−1.38	0.12	0.04
HD 144872	78913	42.55	0.02	8.580	1.038	0.015	−0.64	0.18	0.15
HD 145417	79537	72.01	0.01	7.530	0.940	0.015	−1.39	0.34	0.11
HD 154577	83990	73.41	0.01	7.395	0.980	0.015	−0.63	0.17	0.15
BD+41 3306	94931	28.03	0.03	8.870	0.913	0.015	−0.62	0.17	0.15
HD 193901	100568	22.78	0.04	8.644	0.680	0.008	−1.00	0.15	0.07
BD+24 4460	107314	22.16	0.07	9.463	0.854	0.015	−0.89	0.28	0.15
HD 216259	112870	46.99	0.02	8.294	0.944	0.015	−0.63	0.27	0.15

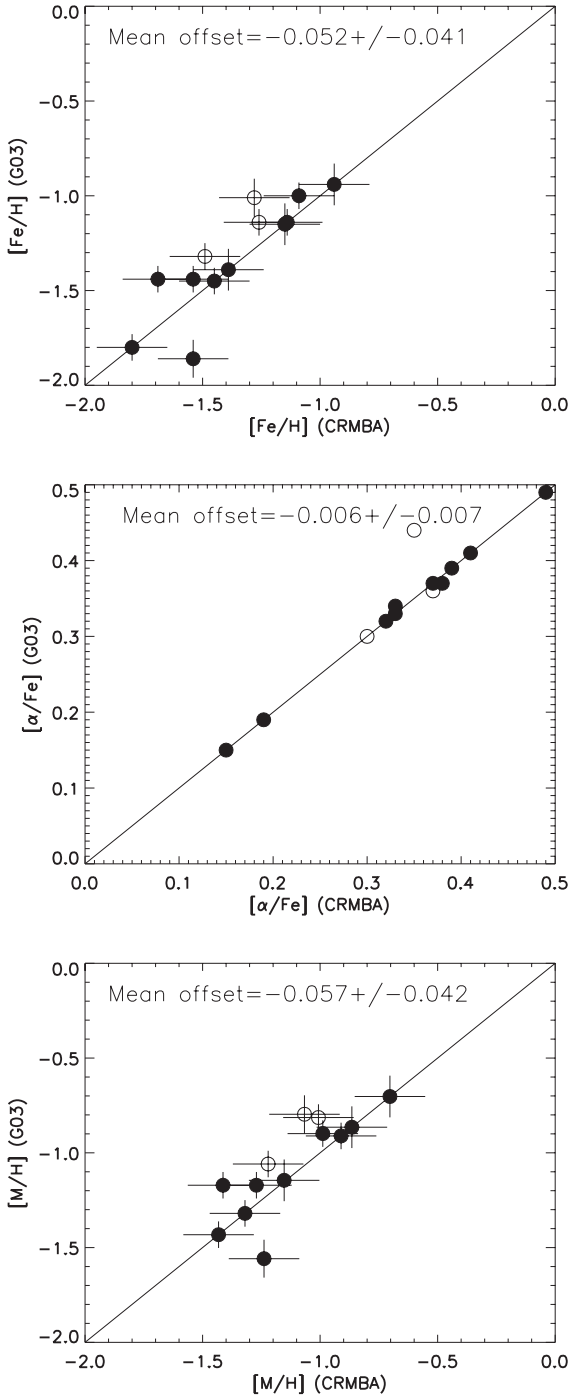

Figure 1. Comparison of [Fe/H] (top), [α/Fe] (middle) and [M/H] (bottom) values from CRMBA versus Gratton et al. (2003a) for the 13 stars in common between the two studies. Bona fide single unevolved subdwarfs are plotted as filled circles, and the mean offsets given in each plot are in the sense (CRMBA–Gratton) and have been calculated based on all stars in the figure.

We now describe our analysis of the final subdwarf sample, consideration of the relevant uncertainties and statistical biases, and the method used to fit our final set of subdwarfs to the target clusters.

2.3 Analysis of the final subdwarf sample

2.3.1 Lutz–Kelker corrections

In order to assess Lutz–Kelker corrections to the absolute magnitudes of the subdwarfs, we plot the proper motion and parallax distributions of all stars from CRMBA with $-2.5 <$ [Fe/H] < -0.5 and $(V - I_C)$ colours in Fig. 3. Following Hanson (1979), Lutz–Kelker corrections can be calculated as a function of the parallax error and n, where $n = x - 1$ and x is the slope of the proper motion distribution, shown in the upper panel of Fig. 3. However, from the parallax distribution, shown in the bottom panel of Fig. 3, we can see that the power-law portion of the proper motion distribution would overestimate Lutz–Kelker corrections for stars with parallaxes $\pi <$ 25 mas, or 12 of the 27 subdwarfs in our final sample. Alternatively, we could apply the corrections from Carretta et al. (2000) and Gratton et al. (1997) for the stars also present in those samples, as done by Gratton et al. (2003a), but these corrections could be inconsistent with those for stars in only the CRMBA sample. For these reasons, we have chosen not to apply Lutz–Kelker corrections to the absolute magnitudes which we derive for our subdwarfs. As we discuss below, this choice has a negligible influence on our results, owing largely to the fact that 18 of our 27 subdwarfs have $\sigma_\pi/\pi \leq 0.05$.

2.3.2 Subdwarf colour corrections

Following the strategy of Carretta et al. (2000), the subdwarfs which were fit to each cluster fiducial sequence were only those with a metallicity [M/H] within $\pm$ 0.5 dex of the cluster [M/H] value. However, since there is only one subdwarf in our final sample with [M/H] < -1.5, four additional subdwarfs with metallicities ranging up to [M/H] $= -1.32$ were used in the fitting for the most metal-poor clusters.[2] In this way, five subdwarfs were used to fit all clusters with [M/H] ≤ -2.0 and for the remainder of the clusters, the number of subdwarfs used for the main-sequence fitting varied between 7 and 23.

For each subdwarf fit to a given cluster, the subdwarf colour was corrected to the value it would have at the cluster metallicity. For the sole purpose of using the cluster fiducial sequences themselves to determine this colour correction, we assume the GGC distances given by D10 so that the cluster fiducial sequences can be shifted from apparent $F814W$ to absolute M_{814} magnitudes. Once this is accomplished, a second-order polynomial is fitted to the main-sequence colour as a function of [M/H] at the absolute M_{814} magnitude of the subdwarf. This procedure has the advantage that it does not require assumptions regarding the constancy of the main-sequence slope as a function of metallicity and/or absolute magnitude. The metallicity uncertainty is transformed to a colour uncertainty using the difference in colour correction that would be obtained if the cluster and subdwarf metallicities were altered by their one sigma uncertainties, and this colour error propagates into a magnitude error using the slope of the main sequence at the magnitude and metallicity of the subdwarf. However, this uncertainty as well as the colour correction itself is minimized due to both the precision of the cluster and subdwarf abundances ($\sigma_{[M/H]} \leq 0.15$ dex) and the restriction of the subdwarf metallicities to values close to the cluster metallicity. Although the assumption of the D10 distance moduli to calculate the colour corrections is somewhat arbitrary, the impact of any discrepancies in these values

[2] To address the lack of metal-poor subdwarfs with accurate parallaxes, one of us (A. Sarajedini) is involved in a programme which is currently obtaining precise *HST* parallaxes for a sample of metal-poor subdwarfs.

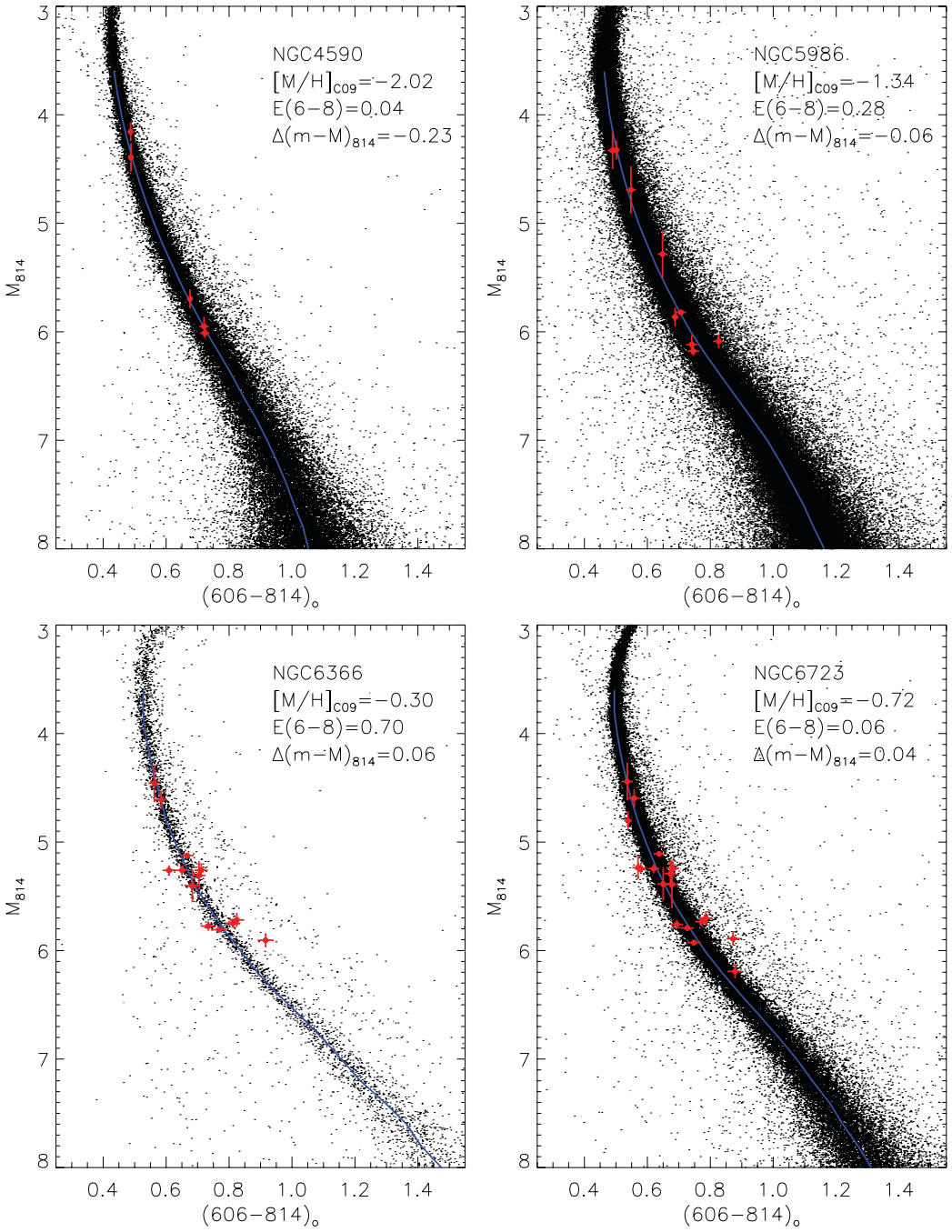

Figure 2. Examples of our subdwarf fits for four clusters with a range of metallicity and reddening values. Small black points represent the ACS photometry, and the fiducial sequence fit to each cluster is shown as a blue line from $M_V = 4.5$ faintward. The fit subdwarfs are shown as red circles with corresponding error bars, and the parameters used for the fit are given in each plot.

is minimal since the maximum colour correction that was applied is 0.053 mag, and the mean absolute value of the colour corrections is <0.01 mag.

2.3.3 *Main-sequence fitting procedure*

The procedure adopted to fit subdwarfs to the fiducial sequence of each cluster was as follows. First, the fiducial sequence of each cluster was dereddened using the $E(6–8)$ reddening value given by D10. Next, the subdwarf-based $F814W$ distance modulus was calculated using a non-linear least-squares fit to minimize the differences between the fiducial $F814W$ magnitudes and those of the subdwarfs, at the colours of the subdwarfs, corrected for metallicity as described above. The total magnitude error for each individual subdwarf, represented by the vertical error bars in Fig. 2, is the sum in quadrature of the magnitude error resulting from uncertainties in subdwarf parallaxes, photometry and the subdwarf and cluster metallicity. These individual errors were used to weight the subdwarfs when performing the non-linear least-squares fit to the fiducial sequences. The formal uncertainties resulting from the least-squares fit range from 0.012 to 0.036 mag among the 46 clusters which were fit, with a mean of 0.020 and a median of 0.017.

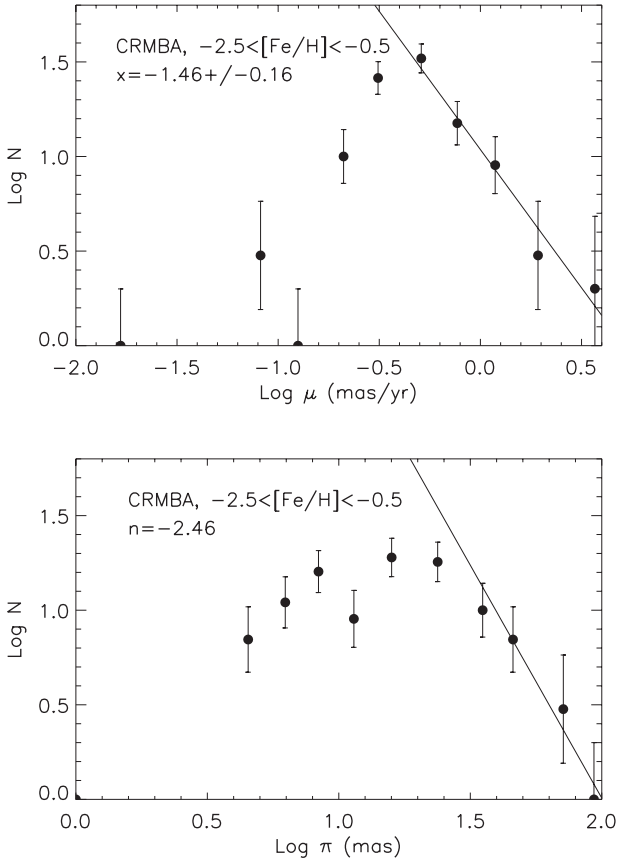

Figure 3. Proper motion (top) and parallax (bottom) distributions for all stars in CRMBA with $-2.5 < [\mathrm{Fe/H}] < -0.5$ and $(V - I)$ photometry. For stars with $\pi \lesssim 25$ mas, Lutz–Kelker corrections based on the power-law slope of the proper motion distribution are overestimated.

2.4 Distances obtained from main-sequence fitting

The $F814W$ distance moduli which we obtain from the subdwarf fits are given in Table 2, along with the adopted reddening from D10. For purposes of comparing these subdwarf-based GGC distance moduli with the isochrone-based GGC distance moduli of D10, we define the quantity $\Delta(m - M)_8$ as the difference between the subdwarf-based $F814W$ distance modulus listed in Table 2 and the value of $(m - M)_8$ given in table 2 of D10, in the sense (D10-Subdwarfs). We find that $\Delta(m - M)_8$, averaged across all 46 clusters which were fit, has a mean value of $-0.094 \pm 0.014(\sigma_{\bar{x}})$. This result is quite insensitive to the choice of Lutz–Kelker corrections or subdwarf colour corrections used. For example, application of Lutz–Kelker corrections based on Fig. 3 changes the mean value of $\Delta(m - M)_8$ by 0.005 mag. Similarly, if, rather than using empirical colour corrections derived from the cluster fiducial sequences, we use colour corrections derived from the Victoria-Regina stellar models (VandenBerg, Bergbusch & Dowler 2006) or the Dartmouth Stellar Evolution Database (Dotter et al. 2008), the mean value of $\Delta(m - M)_8$ changes by -0.033 or -0.002 mag, respectively.

We now discuss the photometric and pulsational properties of SX Phe in GGCs, proceeding under the assumption that the D10 distance moduli are correct to within their <0.1 mag dispersion from our subdwarf-based distance moduli. There are a handful of clusters hosting SX Phe which D10 exclude from their table 2 because they were excluded from the horizontal branch analyses in that study due to the presence of multiple populations. However, as part of their investigation, distance moduli and reddening values were calculated from isochrone fits (A. Dotter, private communication). For the sake of homogeneity, we employ those values here for clusters which host SX Phe but are not listed in table 2 of D10.

Table 2. Globular cluster $F814W$ distance moduli from subdwarf fits.

Cluster	$E(6–8)^a$	DM8(SD)^b	Cluster	$E(6–8)$	DM8(SD)
ARP 2	0.100	17.63	NGC 6218	0.178	13.96
NGC 104	0.010	13.29	NGC 6254	0.248	14.21
NGC 288	0.000	14.80	NGC 6304	0.460	14.78
NGC 1261	0.000	16.06	NGC 6341	0.018	15.03
NGC 1851	0.020	15.42	NGC 6352	0.240	14.15
NGC 2298	0.224	15.55	NGC 6362	0.057	14.58
NGC 3201	0.255	13.98	NGC 6366	0.705	13.94
NGC 4147	0.005	16.60	NGC 6397	0.170	12.67
NGC 4590	0.043	15.53	NGC 6541	0.105	14.83
NGC 4833	0.340	14.93	NGC 6584	0.065	15.95
NGC 5024	0.010	16.66	NGC 6637	0.150	15.05
NGC 5053	0.008	16.56	NGC 6656	0.350	13.43
NGC 5272	0.005	15.13	NGC 6681	0.085	15.17
NGC 5286	0.250	15.84	NGC 6723	0.060	14.63
NGC 5466	0.010	16.39	NGC 6752	0.040	13.35
NGC 5904	0.020	14.44	NGC 6779	0.235	15.86
NGC 5927	0.380	15.38	NGC 6809	0.100	14.01
NGC 5986	0.282	15.79	NGC 6838	0.210	13.43
NGC 6093	0.200	15.68	NGC 6934	0.095	16.34
NGC 6101	0.100	16.28	NGC 6981	0.035	16.24
NGC 6144	0.435	15.56	NGC 7078	0.070	15.64
NGC 6171	0.405	14.40	NGC 7089	0.035	15.55
NGC 6205	0.006	14.52	NGC 7099	0.040	15.09

[a] $E(F606W - F814W)$ reddening adopted from D10.
[b] $F814W$ distance modulus determined from subdwarf fitting.

3 SX PHE PROPERTIES

3.1 The updated SX Phe catalogue

To compile a current list of SX Phe in GGCs, we began with the catalogue of Rodríguez & López-González (2000), which was updated by S01. We then added to this list all SX Phe in GGCs found in the literature since the publication of those studies. This more than doubled the number of SX Phe in GGCs, from 117 listed by S01 to 263 currently known. For the sake of homogeneity, we have excluded the small number of SX Phe in E 3, IC 4499 and Ruprecht 106 from our analysis because isochrone fits to those clusters were not performed by D10. In addition, we have excluded all stars from the original Rodríguez & López-González (2000) catalogue which were also excluded by S01, as well as all SX Phe in NGC 3201 and 4372 due to high differential reddening (Gerashchenko, Kadla & Malakhova 1999; Piersimoni, Bono & Ripepi 2002).

In Table 3, we list all known SX Phe in GGCs by host cluster, along with their primary periods, amplitudes, mean magnitudes, colours and identification of their pulsational modes. Detailed notes regarding pulsational and/or photometric properties of individual SX Phe, and their sources, are given by cluster in Appendix A.

We also address extragalactic SX Phe stars in Local Group star clusters and dwarf galaxies in our subsequent analyses for comparison with GGC SX Phe. In addition to the sources of their pulsational and photometric properties given in Section 1, we give in Table 4 the values and sources of the reddenings and distance moduli which we adopt to place extragalactic SX Phe on colour–magnitude and

Table 3. SX Phe in Galactic globular clusters.

Cluster	Star	log P (d)	A_V (mag)	$\langle V \rangle$ (mag)	$\langle B-V \rangle$ (mag)	$\langle V-I \rangle$	Mode[a]
NGC 104	V1	−1.199	0.15	15.59	0.32		dr
NGC 104	V2	−0.991	0.15	15.07	0.39	0.43	dr
NGC 104	V3	−1.254	0.08	15.93	0.32	0.38	nr
NGC 104	V15	−1.479	0.04	15.28	0.14	0.24	nr
NGC 104	V16	−1.449	0.03	15.76	0.25	0.38	nr
NGC 288	V7	−1.398	0.06	17.92	0.28		u
NGC 288	V6	−1.173	0.41	17.28	0.30		u
NGC 288	V4	−1.102	0.30	17.24	0.29		u
NGC 288	V9	−1.405	0.05	17.52	0.29		u
NGC 288	V8	−1.333	0.06	17.78	0.28		u

Table 3 is available in its entirety electronically (see Supporting Information). A portion is shown here for guidance regarding its form and content.
[a] dr = double radial modes, nr = non-radial modes, fnr = fundamental and non-radial modes, mp = multiperiodic, u = unknown.

Table 4. Local Group SX Phe populations.

Target	N(SX)	$E(B-V)$	$(m-M)_0$	Reference
Fornax DSph	44	0.02 ± 0.01	20.72 ± 0.04	Rizzi et al. (2007)
Fornax 5	1	0.05 ± 0.01	20.70 ± 0.05	Greco et al. (2009), Mackey & Gilmore (2003)
Carina	14	0.05 ± 0.03	20.10 ± 0.02	Pietrzynski et al. (2009), Smecker-Hane, Stetson & Hesser (1994)
Leo IV	1	0.04 ± 0.01	20.95 ± 0.03	de Jong et al. (2008), Belokurov et al. (2007)
LMC	63[a]	0.137 ± 0.05	18.47 ± 0.14	NED[b]
NGC 2155	2	0.169 ± 0.015	18.50 ± 0.13	Otulakowska et al. (2011)
IC 1613	5	0.025 ± 0.01	24.40 ± 0.07	Bernard et al. (2010)

[a] This is the number of fundamental and first-overtone double radial mode δ Scuti detected in the LMC in the OGLE-III data base (Poleski et al. 2010).
[b] Because distance estimates to the LMC are so numerous, we use the mean and standard deviation given in the NASA Extragalactic Database, at http://nedwww.ipac.caltech.edu.

period–luminosity diagrams. In addition, we include the double radial mode δ Scuti in the LMC from the OGLE-III catalogue (Poleski et al. 2010) which we have corrected for differential reddening using the reddening map of Nikolaev et al. (2004) assuming $A_V = 3.24E(B-V)$ (Soszynski et al. 2003) and for geometrical effects following Harris & Zaritsky (2009). The photometry of the two SX Phe in the LMC cluster NGC 2155 has been dereddened using the distance modulus and extinction law employed by Otulakowska et al. (2011). For this cluster and the LMC δ Scuti, the reported amplitudes A_I have been converted to A_V assuming an amplitude ratio of $A_V/A_I = 1.9$ from Rodríguez et al. (2007).[3]

3.2 Colour–magnitude diagrams

We use the colours and apparent magnitudes in Table 3 in combination with cluster distance moduli and reddenings from D10 to test the hypothesis that all SX Phe in GGCs are blue stragglers. We have excluded SX Phe with uncertain colours (see Appendix A). It is worth noting, in the context of colour–magnitude diagrams as well as the period–luminosity relations discussed in the next section, that despite the calibration of time series photometry to the standard magnitude system, sizeable discrepancies in mean magnitude and/or colour can still be found in cases where the same cluster was monitored in separate investigations. For example, the V magnitudes reported for V2 and V15 in 47 Tuc differ significantly beyond their reported photometric errors between the studies of Gilliland et al. (1998) and Bruntt et al. (2001).

Colour–magnitude diagrams in the (M_V, $B-V$) and (M_V, $V-I$) planes are shown in Fig. 4, where different symbols correspond to different pulsational modes as given in the last column of Table 3. Isochrones and zero-age main sequences (ZAMS) from the Dartmouth Stellar Evolution Database (Dotter et al. 2008) corresponding to [α/Fe] = 0.4 and [Fe/H] = −0.5 and −2.5, essentially bracketing the metallicity range occupied by GGCs, have been overplotted. In addition, the dashed lines indicate the empirical δ Scuti instability strip from Rodríguez & Breger (2001), transformed to the Johnson–Cousins filter system using the coefficients of Caldwell et al. (1993). The metal-poor nature of GGC SX Phe is evidenced by the extent of the distribution blueward and faintward of the [Fe/H] = −0.5 ZAMS, and we confirm the finding of Rodríguez & Breger (2001) that SX Phe tend towards the cool side of the instability strip.

The colours for SX Phe variables in M3 (NGC 5272) reported by Nemec & Park (1996) may be significantly erroneous, since the location of the variable NW449, at $(B-V)_0 \sim 0$, is 0.1 mag bluer and 0.5 mag fainter than the ZAMS corresponding to the most metal-poor GGCs ([Fe/H] = −2.5). The double radial mode variable V99 is unusually blue as well, and based on its pulsational properties, Arellano Ferro et al. (2011) suggest that it may be a binary or photometric blend, which would be consistent with its small pulsational

[3] This value is based on fig. 7 of Rodríguez et al. (2007), and their Sections 5.2 and 5.3 imply that this value should be relatively insensitive to changes in $T_{\rm eff}$ and $\log g$. However, these amplitudes should still be regarded as somewhat uncertain, especially in the case of the high-amplitude SX Phe in NGC 2155.

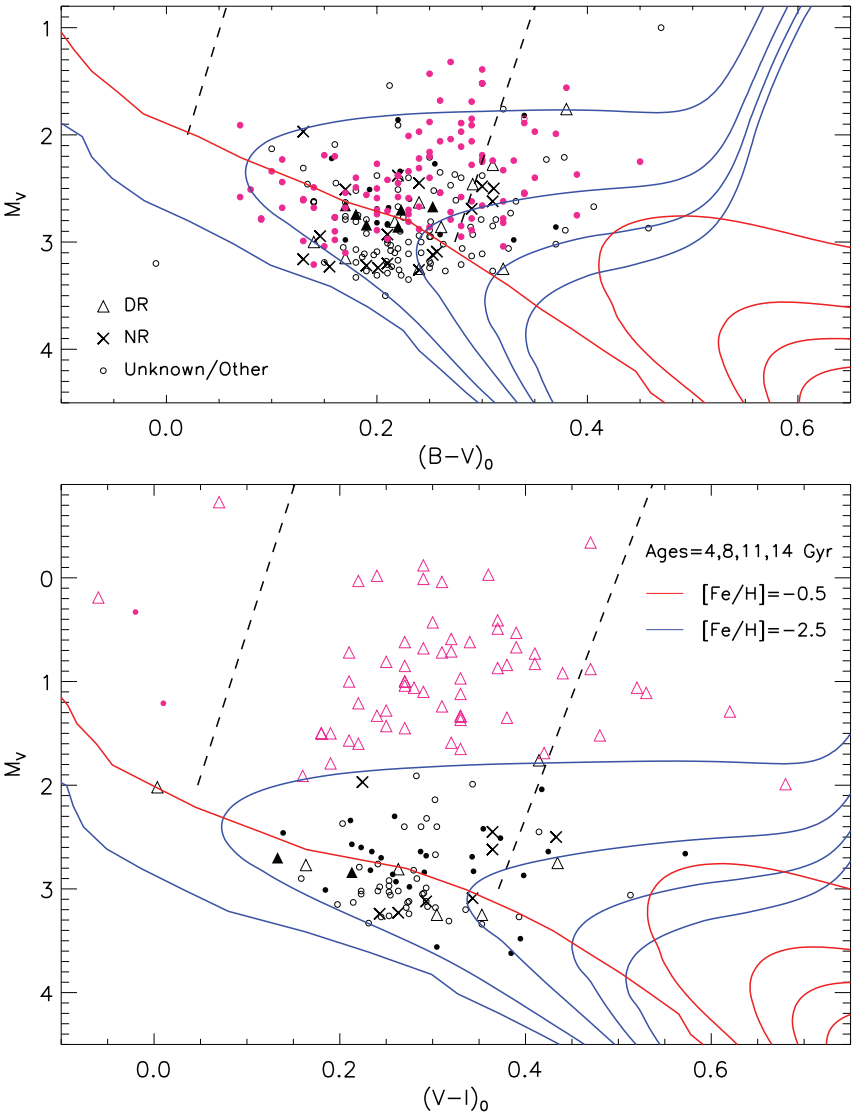

Figure 4. $(B - V)$ (top) and $(V - I)$ (bottom) colour–magnitude diagrams for the SX Phe in our catalogue. Variables with uncertain colours (indicated in Appendix A) have been excluded. Double radial (DR) mode pulsators are indicated by triangles, non-radial (NR) by crosses, and all other SX Phe are plotted with circles. SX Phe in GGCs are black and extragalactic SX Phe (including LMC δ Scuti) are magenta. Open symbols are variables with $A_V \leq 0.2$ and filled symbols indicate $A_V > 0.2$. The location of the ZAMS and 4, 8, 11 and 14 Gyr isochrones are shown for [Fe/H] $= -0.5$ (red) and [Fe/H] $= -2.5$ (blue). The dashed lines indicate the location of the empirical δ Scuti instability strip from Rodríguez & Breger (2001). For clarity, this figure is available in colour in the electronic version of this journal.

amplitude. The two SX Phe in the LMC cluster NGC 2155 are unusually blue and bright, and Otulakowska et al. (2011) were unable to reconcile their pulsational and photometric properties save for the suggestion of a significant helium enhancement. While we will return to this idea in Section 4, it is also possible, although unlikely, that these stars, as well as the two extremely blue double radial-mode LMC variables, may be foreground δ Scuti, in which case reduced distance moduli and extinction would place them plausibly within the δ Scuti instability strip. Of the four unusually red SX Phe, three are in ω Cen: NV328 from Olech et al. (2005), which they mention as being the reddest SX Phe in their sample, along with V92 and V131 from Weldrake, Sackett & Bridges (2007). These latter two SX Phe may not be cluster members since they lie ∼20 arcmin from the cluster core, at nearly four times the cluster half-light radius given by Harris (1996, 2010 revision). In the case of V92, which has $(V - I)_0 = 0.89$, it is unlikely that differential reddening could be responsible for the colour discrepancy even given the fact that ω Cen exhibits significant abundance variations (e.g. Marino et al. 2010; Dupree, Strader & Smith 2011). V101 in NGC 2419 is unusually red as well, but there is no evidence to suggest that the photometry of this star (Di Criscienzo et al. 2011) is suspect.

We also investigate whether high-amplitude ($A_V > 0.2$) SX Phe occupy a narrow subregion of the instability strip compared to their lower amplitude counterparts, as is the case with Galactic high-amplitude δ Scuti (PCD99). To this end, we plot in Fig. 5 SX Phe amplitude versus the distance in (dereddened) colour from the empirical red edge of the δ Scuti instability strip (DSRE) taken from Rodríguez & Breger (2001). We have excluded extragalactic SX Phe from this plot since their larger minimum detectable amplitude and photometric errors likely mask any trend in their colour as a function of amplitude. However, among the GGC SX Phe, it is evident from Fig. 5 that like their δ Scuti cousins, the width of the SX Phe colour

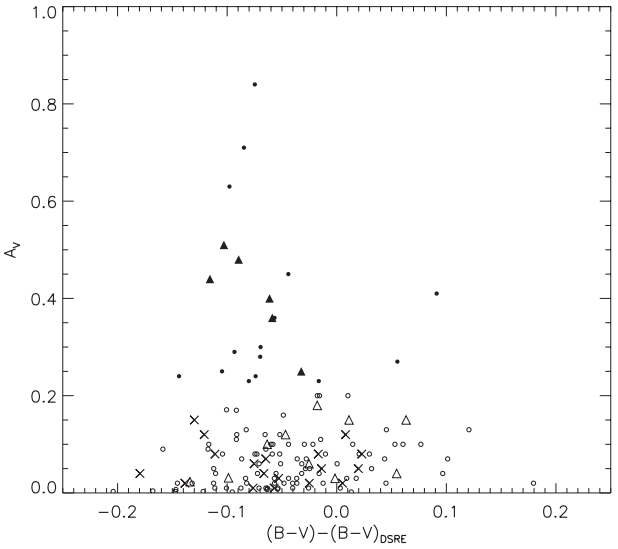

Figure 5. Amplitude versus distance in $(B - V)$ colour from the empirical δ Scuti instability strip red edge (DSRE) for SX Phe in GGCs. Symbols are as in Fig. 4 and stars with uncertain amplitudes and/or colours have been excluded.

distribution within the instability strip decreases substantially with increasing pulsation amplitude.

To confirm that all SX Phe in GGCs are blue stragglers, we plot the GGC SX Phe in Fig. 4 with colours and magnitudes shown relative to the location of the turn-off in their respective host clusters in Fig. 6. Turn-off colours and magnitudes were determined using isochrones from the Dartmouth Stellar Evolution Database (Dotter et al. 2008), calculated as the bluest point on the isochrone generated using the best-fitting age, metallicity and α enhancement values given by D10. The symbols corresponding to the various pulsation modes and ZAMS in this plane are the same as in Fig. 4, and the approximate location of the blue straggler region as defined by the turn-off colour and magnitude is demarcated with a dotted line. The SX Phe in NGC 2419 are excluded from the top panel of Fig. 6 since D10 do not give an age for that cluster. The lack of SX Phe stars within ∼0.5 mag of the turn-off is at least partially an artefact of the photometric biases inhibiting blue straggler (and hence SX Phe) selection and identification due to the fact that fainter blue stragglers, which have larger photometric errors, are also redder and therefore more easily confused with turn-off stars. It is clear from Fig. 6 that, aside from the few outliers mentioned above, all known SX Phe in GGCs are blue stragglers based on their locations relative to the turn-off in their respective host clusters. With this information in hand, we may use period–luminosity relations to investigate potential astrophysical differences between the blue straggler SX Phe in GGCs and the predictions of models based on single-star evolution.

3.3 Mode identification

Pulsation modes must be reliably identified to construct accurate period–luminosity relations since these relations depend on pulsation mode (e.g. S01; Templeton et al. 2002; Olech et al. 2005). Because non-radial modes are commonly observed in SX Phe (e.g. Pych et al. 2001; Olech et al. 2005), secure identification of pulsation modes is often difficult, especially in the case where only one pulsation mode is observed. This problem is exacerbated by the fact that the non-radial modes have been observed to cluster near radial modes in frequency space for at least one field SX Phe (Rodríguez et al. 2007) as well as some δ Scuti (Breger, Lenz & Pamyatnykh 2009). Observationally expensive solutions to this problem do exist, including the use of phase shifts and amplitude ratios from multiband time series photometry (Daszyńska-Daszkiewicz 2008), time series spectroscopy (e.g. Castanheira et al. 2008) and secular period changes (S01). However, the distance and/or concentration of GGCs and Local Group dwarf galaxies has thus far rendered these methods impractical.

We have analysed our updated catalogue of SX Phe to search for a means by which we can confidently identify the pulsation modes of a large enough sample of pulsators to compare observed and theoretical period–luminosity relations. Location in the colour–magnitude diagram does not provide any reliable information regarding pulsation mode, at least to within observational uncertainties, as evidenced by Fig. 4. While large pulsation amplitude and/or light-curve asymmetry have been used as hints of fundamental radial mode pulsations, models of δ Scuti imply that neither of these features are unique to the fundamental radial mode and can misidentify overtone pulsators (Bono et al. 1997; Templeton, Guzik & McNamara 1998). However, certain trends are visible in the pulsational properties of the SX Phe in our updated data base. For example, there are no non-radial pulsators with $A_V > 0.15$, whereas radial pulsators tend to have larger amplitudes, and we address the use of amplitude to select radial pulsators in the next section. In any case, amplitude alone cannot be used as a reliable discriminant between radial and non-radial pulsators since there are double radial mode pulsators with $A_V < 0.15$, as well as probable additional fundamental mode SX Phe which are not double radial mode pulsators. Similarly, light-curve asymmetry alone is not a sufficient criterion for mode identification since there are many probable radial pulsators which have sinusoidal light curves (e.g. Olech et al. 2005). Analysis of the Fourier components of SX Phe light curves, in addition to requiring hundreds of high signal-to-noise ratio observations, suffers from the photometric bias that lower amplitude pulsators will have poorly constrained Fourier parameters.

All recent SX Phe pulsation models are in good agreement on the narrow range of period ratios which result from the excitation of multiple radial pulsation modes (Gilliland et al. 1998; S01; Templeton et al. 2002; Olech et al. 2005). For this reason, multimode pulsators are the best prospects for secure mode identification using their period ratios. Hence, we initially use multimode radial pulsators to construct an empirical period–luminosity relation for comparison with predictions from single-star models. More specifically, we select fundamental and first-overtone multimode radial pulsators and use them to construct a fundamental mode period–luminosity relation. We choose the fundamental mode for two reasons. First, it is likely the most common radial mode in our sample, at least at observable amplitudes, as we discuss in the next section. Secondly, we wish to compare our observed period–luminosity relation with those predicted by pulsational model grids (PCD99 and PF02) as well as the recent empirical relation of P08, all of which are calculated only for the fundamental radial mode.[4]

[4] Although the SX Phe models of Olech et al. (2005) and S01 cover a smaller area of parameter space than those of PF02 and PCD99, they suggest that period–luminosity relations for higher order radial modes are parallel (Olech et al. 2005), or nearly parallel (S01), to the fundamental mode period–luminosity relation.

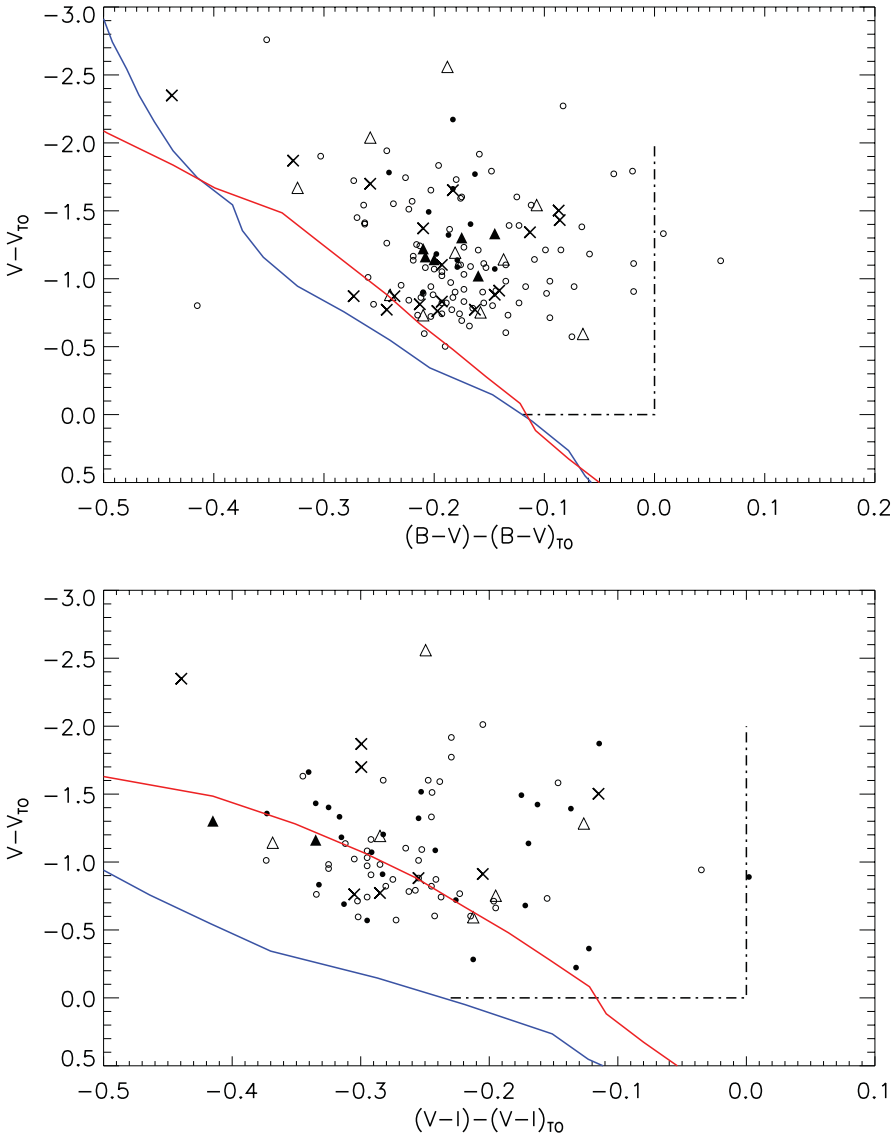

Figure 6. Colour–magnitude diagrams for SX Phe in GGCs, plotted relative to the colour and magnitude of the main-sequence turn-off in their respective host clusters. Symbols are as in Fig. 4, including the location of the ZAMS corresponding to [Fe/H] = −0.5 and −2.5 in this plane. The dot–dashed lines indicate the blue straggler region as demarcated by the turn-off colour and magnitude.

3.4 SX Phe period–luminosity relations

Our goal is to use period–luminosity relations to explore the hypothesis that the pulsational properties of blue stragglers can be used to constrain their evolutionary histories. This may be accomplished via comparison of observed GGC SX Phe (i.e. blue straggler) relations to those predicted by normal single star pulsation and evolutionary models.

All recent SX Phe pulsational model grids (S01; PF02; Olech et al. 2005) are in agreement that the inclusion of colour and/or metallicity terms, resulting in a period–luminosity–colour–metallicity relation (PLCZR), greatly reduces the intrinsic dispersion of the relation by a factor of up to 8 (PF02). However, when fitting period–luminosity relations to SX Phe in GGCs, we find, in agreement with P08, that insignificant colour and/or metallicity terms result when they are included in a non-linear least-squares fit. Hence, we use simpler, linear relations, at the cost of precision. As discussed by P08, the advantage of this form of the relation is that it does not require any assumptions regarding metallicity, which is useful in the case of Local Group galaxies with non-trivial star formation histories (e.g. Fornax, see Coleman & de Jong 2008). We initially perform a linear least-squares fit to only those SX Phe in GGCs which are double radial mode pulsators to avoid misidentifying pulsation modes. However, because there are only 21 such variables, the resulting relation suffers from large uncertainties in its coefficients. If we surmise that all high-amplitude ($A_V > 0.2$) SX Phe are radial pulsators, then we may augment the sample by including all 'predicted' fundamental radial mode SX Phe, or in other words, those high-amplitude SX Phe which have M_V residuals within the one-sigma dispersion of our double radial mode relation. This increases the number of stars from 21 to 77, and we then obtain

$$M_V = -1.640 - 3.389 \log P_f \quad \sigma = 0.104 \pm 0.110 \pm 0.090. \tag{1}$$

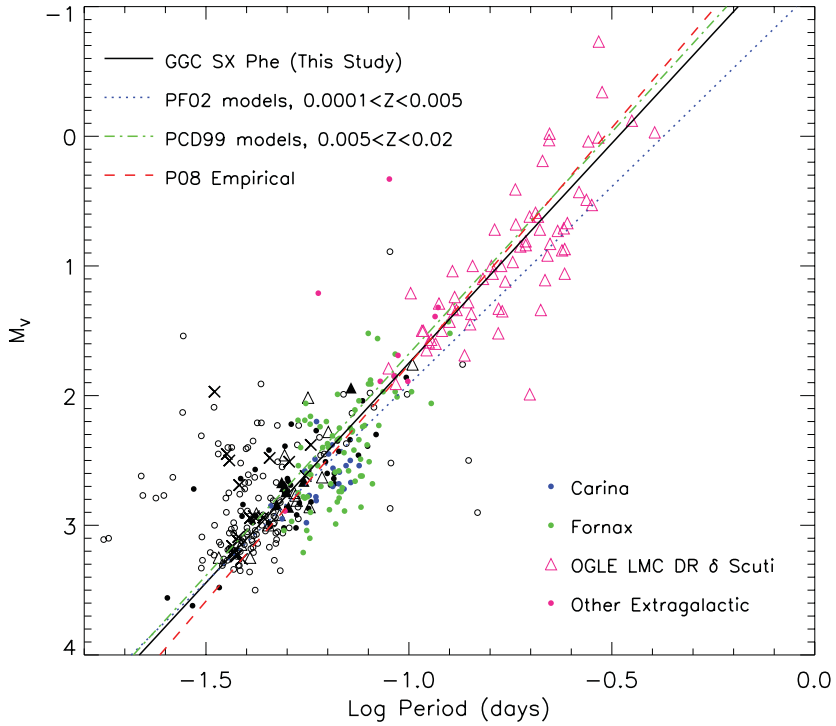

Figure 7. Period–luminosity relations for our sample. Symbols are the same as in the previous two figures except that the extragalactic SX Phe in Fornax and Carina are now plotted in blue and green, respectively. The solid black line corresponds to our relation based on SX Phe in GGCs, the blue dotted line corresponds to the theoretical SX Phe relation from PF02, the green dot-dashed line to the predicted δ Scuti relation from PCD99, and the red dashed line to the empirical relation of P08.

The inclusion of the additional high-amplitude SX Phe changes the coefficients by <2 per cent, strongly suggesting that GGC SX Phe with $A_V > 0.2$ are unlikely to be non-radial pulsators, in accord with the low observed amplitudes of multimode non-radial pulsators.[5] The remaining scatter in equation (1) is likely due to photometric calibration uncertainties between the variety of photometric time series investigations included in our catalogue. To investigate whether differential reddening also contributes significantly to this scatter, we attempted to construct reddening-independent period–Wesenheit relations using all the GGC SX Phe in our catalogue for which colours are available. Although some degree of differential reddening is more the rule than the exception for GGCs (e.g. D10; Milone et al., in preparation), the uncertainties of the coefficients in the resulting W_{BV} and W_{VI} relations revealed no improvement over equation (1), implying that differential reddening is not the primary contributor to the scatter in our period–M_V relation. We now compare equation (1) with theoretical predictions for single stars, and use extragalactic SX Phe and δ Scuti as a test of these relations.

3.5 Comparison with extragalactic SX Phe

It has been shown that distance determinations may be provided by high-amplitude δ Scuti (PCD99; McNamara, Clementini & Marconi 2007) and/or SX Phe (McNamara 1997; McNamara et al. 2004) if their pulsation modes could be securely determined. From a practical standpoint, a single relation which can be applied to SX Phe or δ Scuti in this context, while requiring a sacrifice of precision due to the lack of colour and metallicity terms, would be most broadly applicable to extragalactic populations. In Fig. 7, we plot equation (1) to compare the pulsational properties of blue stragglers (on which the relation is based) to theoretical predictions based on normal single stars. To this end, we show the linear relations predicted by the low-metallicity pulsational model grid of PF02 ($0.0001 \leq Z \leq 0.005$) and the high-metallicity grid of PCD99 ($0.005 \leq Z \leq 0.02$), along with the empirical relation derived by P08 based on a combination of GGC, Milky Way field, and Local Group variables.[6] In addition, we plot all known SX Phe in the Local Group as well as LMC δ Scuti to assess whether equation (1) can be employed to determine distances without requiring a priori assumptions regarding metallicity. The cause of the scatter seen in the LMC double radial mode δ Scuti, identified as such in the OGLE-III data base based on their period ratios (Poleski et al. 2010), may be ascribed to several phenomena. In addition to residual small-scale reddening variations, the aforementioned tendency of non-radial modes to occur near radial modes could result in the misclassification of some δ Scuti which are actually exhibiting a mix of radial and non-radial modes. In addition, their period ratios could be affected by rotation (e.g. Suárez, Garrido & Goupil 2006), possibly scattering true double radial mode pulsators out of the accepted period ratio range and vice versa. Rotation could also explain the disagreement between observed and predicted period ratios for well-studied double radial

[5] Importantly, this is not to say that all high-amplitude SX Phe are *fundamental mode* radial pulsators, which is why we used only F/1OT double radial mode pulsators as a guide to select additional (probable single-mode) fundamental mode SX Phe and exclude radial overtone pulsators.

[6] We have shifted the P08 relation brightward by 0.06 mag to account for the difference between our assumed distance moduli and theirs for M55, ω Cen and the LMC. The value of 0.06 is the mean difference in assumed distance moduli for these three populations, weighted by the number of stars in the P08 sample in each population.

mode SX Phe in GGCs such as V41 in M55 (Pych et al. 2001) and V2 in 47 Tuc (Bruntt et al. 2001).

It is clear from Fig. 7 that all of the period–luminosity relations are in reasonable agreement over the period range of the GGC SX Phe. It is perhaps not surprising that our relation (equation 1) is in good agreement with the the empirical relation of P08, except at the extreme short-period end of the SX Phe period distribution ($\log P < -1.5$), possibly due to their inclusion of the Fornax and Carina SX Phe and the then-available data base of LMC δ Scuti to calculate their fit. Most notably, our empirical relation fits the LMC δ Scuti well while the relation of PF02 does not. Our relation predicts a dereddened LMC distance modulus of $(m - M)_0 = 18.49 \pm 0.10$ (systematic) $\pm\, 0.04(\sigma_{\bar{x}})$, in excellent agreement with literature estimates (see Table 4) and with newly obtained *HST* parallaxes of five RR Lyrae stars (F. Benedict, private communication). Also, our relation is nearly identical to the linear δ Scuti relation predicted by the metal-rich models of PCD99. The fact that a relation based solely on GGC SX Phe fits the LMC and the metal-rich PCD99 models well is interesting given that 90 per cent of the SX Phe used to calibrate equation (1) reside in clusters with [Fe/H] ≤ -1.5.

We plot the residuals of our fit in Fig. 8 to illustrate that there is a group of high-amplitude 'subluminous' pulsators with magnitudes too faint for their pulsation periods, or to put it another way, periods too long for their luminosities. These SX Phe are unlikely to be non-radial pulsators due to their high amplitudes, and have been noted in the Carina and Fornax dwarf spheroidal galaxies (P08) as well as a few low-amplitude examples in ω Cen (Olech et al. 2005), and we now address them in more detail.

3.6 Origin of the subluminous variables

For the purposes of the following discussion, we define 'subluminous' SX Phe as those which have $A_V > 0.2$ and lie more than 0.2 mag faintward of the relation given in equation (1), as shown in Fig. 8. The latter criterion effectively serves as a 2σ cut to exclude fundamental mode SX Phe. There are several possible explanations for the existence of the subluminous SX Phe.

(1) They are merely a result of assumed distance moduli which are too small by ∼0.2–0.3 mag. In the case of the GGCs, this is unlikely given the agreement between isochrone and subdwarf-based distances discussed in Section 2. However, it is worth noting that because the two GGCs which host the most subluminous variables (NGC 2419 and ω Cen) also have multiple stellar populations, they were not included in the 46 clusters for which subdwarf fitting was done, so a direct subdwarf-based distance is not available. In the cases of Carina and Fornax, recent distance determinations also do not support a significant revision of their distance moduli from the values used here. Various distance determinations for Carina over the last decade, using several different techniques, all yield $20.05 \leq (m - M)_0 \leq 20.17$, with uncertainties of <0.1 mag. Similarly, the largest distance estimates for Fornax are still too small to bring its subluminous SX Phe within the 1σ dispersion of equation (1). However, while statistically unlikely, we cannot completely discard erroneous distance moduli as a possibility.

(2) Binaries or photometric blends cannot be responsible since they would cause a given star to appear too bright at a given period, not too faint. Furthermore, blending would likely result in a smaller observed pulsation amplitude.

(3) The possibility that subluminous variables are indicative of a particular blue straggler formation process, resulting in stars with physical properties distinct from normal single stars, is discussed by P08 in the context of the multiple populations of Fornax. In particular, P08 suggest a smaller stellar radius as a mechanism to explain subluminous SX Phe. This is an interesting theory, and we wish to advance an additional or alternative possibility.

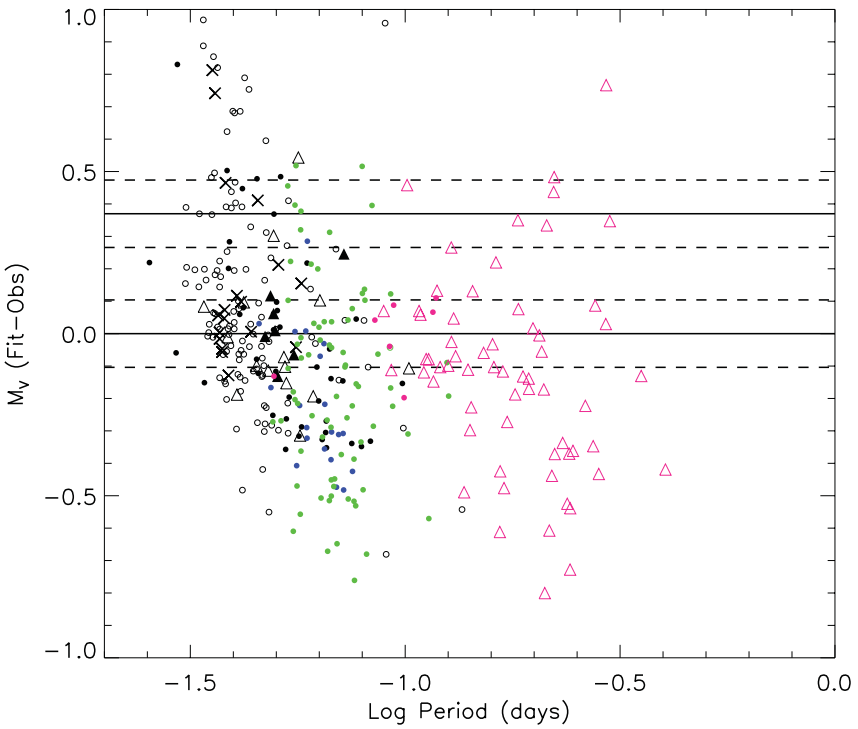

Figure 8. Residuals of our period–luminosity relation from Fig. 7. Symbols are the same as in that figure. The solid lines indicate the locations of the fundamental (lower) and first overtone (upper) radial modes, and the dashed lines indicate the 1σ dispersion of the relation, shown for both modes.

(4) NGC 2419 and ω Cen host more subluminous SX Phe than other GGCs. These two clusters have several other unusual properties in common which they do not share with most GGCs; with respect to the subluminous SX Phe, both of these clusters contain populations with unusually high helium abundances. In the case of NGC 2419, Di Criscienzo et al. (2011) estimate that ∼30 per cent of the cluster population has an initial helium mass fraction close to $Y = 0.42$. For ω Cen, Piotto et al. (2005, and references therein) suggest a value of $Y \geq 0.35$ for ∼25 per cent of the main-sequence stars, although recent RR Lyrae models suggest that the fractional size of the He-enhanced population may be somewhat smaller (Marconi et al. 2011). SX Phe pulsational models predict that a helium enhancement from $Y = 0.23$ to 0.3 will cause an increase in period of ∼20 per cent (S01), corresponding to a magnitude offset of ∼0.27 at fixed log P assuming the slope of equation (1), which is tantalizingly similar to what is observed in Fig. 8. In this context, there are two possibilities: Either subluminous SX Phe are the BSS progeny of helium enhanced second-generation stars, and/or their longer periods are indicative of an enhancement of helium in their envelopes resulting from the BSS formation process itself.

4 DISCUSSION AND SUMMARY

4.1 Helium and the subluminous variables

There is now a substantial body of evidence for a helium spread/enhancement in GGCs, based on red giants (Bragaglia et al. 2010a; Pasquini et al. 2011), light element abundances of dwarfs (Bragaglia et al. 2010b), and GGC horizontal branches (Gratton et al. 2010), but significant challenges to this scenario persist (e.g. Newsham & Terndrup 2007; Catelan et al. 2009). Even if we can safely assume that SX Phe subluminosity has an astrophysical rather than observational origin, as is likely the case at least in Fornax (P08), we are still left with the task of distinguishing between blue stragglers which formed from helium enhanced progenitors (i.e. second generation cluster stars) and blue stragglers whose helium enhancement is a result of the blue straggler formation process. Direct observational evidence for or against a link between subluminous SX Phe and helium enhancement is likely to remain elusive. Although helium abundances have been measured spectroscopically for a handful of hot horizontal branch stars in GGCs (e.g. Moehler et al. 2007; Villanova, Piotto & Gratton 2009) and red giants in ω Cen (Dupree et al. 2011), sufficiently precise spectroscopy at the temperature and luminosity range of the SX Phe instability strip would be extremely challenging. Multicolour photometry may provide some clues, as binary mass transfer models for case A, in which the donor star is on the main sequence, or case B, in which the donor star is on or evolving towards the red giant branch (Kippenhahn & Weigert 1967), predict several observable modifications to the resultant blue straggler due to helium accreted from the donor star. First, the additional helium, which will likely be mixed into the envelope, can shift the colour of the straggler significantly blueward, possibly beyond the helium-normal ZAMS (Chen & Han 2008). Among the subluminous SX Phe, those in M92 (NGC 6341) and, to a lesser extent, ω Cen, have bluer colours than the high-amplitude SX Phe in general (although none of these are bluer than the ZAMS), whereas all four of the subluminous SX Phe in NGC 2419 are quite red. Secondly, blue stragglers resulting from close main-sequence binaries may have a smaller radius, as hypothesized by P08, and CNO abundance abnormalities (Chen & Han 2004), as seen for 14 per cent of the blue stragglers in 47 Tuc examined spectroscopically by Ferraro et al. (2006) but none of the 11 blue stragglers observed in a similar fashion in M4 (Lovisi et al. 2010).

The cases of Carina and Fornax are especially complicated. In addition to the coexistence of young, intermediate age and old populations, existing *HST* time series of Local Group dwarfs only reveal SX Phe with $A_V \gtrsim 0.2$, so that any analysis of their SX Phe suffers from a photometric bias (although our GGC SX Phe catalogue is not entirely free from such biases either, as mentioned in Section 3.2). It is evident from Figs 4 and 7 that less luminous SX Phe tend to have smaller pulsation amplitudes, implying that the limiting detectable amplitude in the Local Group galaxies effectively imposes limits on the periods and absolute magnitudes of SX Phe which can be detected. SX Phe models (S01; Bono et al. 2002) predict that helium enhancement should systematically affect pulsation amplitudes, but extremely time intensive variability studies of Local Group SX Phe would be needed before a comparison between their pulsational properties and those of GGC SX Phe could be made in earnest. While fairly ambitious spectroscopic campaigns targeted at nearby dwarf spheroidals are proving quite fruitful (e.g. Fabrizio et al. 2011, and references therein), disentangling chemical abundances and the dynamical issues involved in blue straggler formation among coexisting multiple-age populations is a daunting task.

An additional caveat is that there is currently no 'normal' (i.e. non-blue straggler) observed population of SX Phe against which metal-poor pulsational models can be compared. The isochrones in Fig. 4 imply that if a young or intermediate-age population could remain extremely metal-poor ([Fe/H] ≈ -2.5 at <8 Gyr), then upper main sequence and turn-off stars would reside in the instability strip, in direct analogy to δ Scuti stars. However, even if such a population could be detected and identified, obtaining time series photometry with the necessary precision would require a huge observational investment.

We are currently addressing the aforementioned issues from a different angle using dynamical simulations of GGCs to investigate blue straggler formation and evolution, and their relationship to cluster physical parameters. The goal is that the simulations may be used to trace the formation histories of individual blue stragglers, providing insight into the dependence of formation mechanism on stellar and cluster properties.

4.2 Summary of results

In closing, we summarize the results of our study as follows.

(1) We have verified the isochrone-fitting distances to 46 GGCs from D10 by fitting their main sequences to a carefully chosen set of nearby ($E(B-V) \leq 0.002, \sigma_\pi/\pi \leq 0.1$), unevolved ($M_V > 5$) subdwarfs. The subdwarf-based distance moduli are consistent with the isochrone fitting distance moduli at the 0.1 mag level in the mean.

(2) We have created an updated catalogue of SX Phe in GGCs and the Local Group. Using this updated catalogue, we confirm that pulsational amplitude or light-curve shape cannot be reliably used to identify a specific pulsation mode. However, all non-radial multimode pulsators have $A_V \leq 0.15$, and high-amplitude ($A_V > 0.2$) SX Phe appear to occupy a narrow subregion of the instability strip and are all likely radial mode pulsators.

(3) We have constructed an empirical period–luminosity relation based on double radial mode SX Phe; this relation is in excellent agreement with model predictions for single, metal-rich ($Z \geq 0.006$) pulsators and the recent empirical relation of P08, yielding an LMC

distance in superb agreement with recent independently determined values. Although the scatter in this relation ($\sigma \simeq 0.1$) is greater than that predicted for relations which include colour and/or metallicity terms, our relation can be applied to extragalactic populations regardless of metallicity.

(4) NGC 2419 and ω Cen both harbour several subluminous SX Phe. We suggest that they may be connected to the unusually high helium abundances suggested for sizeable subpopulations within these clusters. However, this connection and its relationship to blue straggler formation is difficult to confirm observationally. Because many subluminous SX Phe are seen in Carina and Fornax as well, improved chemical abundances or time series data for those galaxies may help resolve whether subluminous SX Phe are due solely to a helium enhancement in their progenitors or whether they are indicative of a particular blue straggler formation channel.

ACKNOWLEDGMENTS

The authors wish to thank D. Majaess for helpful discussions as well as F. Benedict for disclosing the results of newly obtained RR Lyrae parallaxes. This research has made use of the NASA/IPAC Extragalactic Database (NED) which is operated by the Jet Propulsion Laboratory, California Institute of Technology, under contract with the National Aeronautics and Space Administration, as well as the SIMBAD data base, operated at CDS, Strasbourg, France.

REFERENCES

Anderson J., Piotto G., King I. R., Bedin L. R., Guhathakurta P., 2009, ApJ, 697, L58
Arellano Ferro A., Giridhar S., Rojas López V., Figuera R., Bramich D. M., Rosenzweig P., 2008, Revista Mexicana Astron. Astrofisica, 44, 365
Arellano Ferro A., Giridhar S., Bramich D. D., 2010, MNRAS, 402, 226
Arellano Ferro A., Figuera Jaimes R., Giridhar S., Bramich D. M., Hernández Santisteban J. V., Kuppuswamy K., 2011, MNRAS, 416, 2265
Bailyn C. D., 1992, ApJ, 392, 519
Belokurov D. B. et al., 2007, ApJ, 654, 897
Benkő J. M., Bakos G. Á., Nuspl J., 2006, MNRAS, 372, 1657
Bernard E. J. et al., 2010, ApJ, 712, 1259
Bono G., Caputo F., Cassisi S., Castellani V., Marconi M., Stellingwerf R. F., 1997, ApJ, 477, 346
Bono G., Caputo F., Marconi M., Santolamazza P., 2002, Observational Aspects of Pulsating B- and A Stars, 256, 249
Bragaglia A., Carretta E., Gratton R., D'Orazi V., Cassisi S., Lucatello S., 2010a, A&A, 519, A60
Bragaglia A. et al., 2010b, ApJ, 720, L41
Bramich D. M., Figuera Jaimes R., Giridhar S., Arellano Ferro A., 2011, MNRAS, 413, 1275
Breger M., Lenz P., Pamyatnykh A. A., 2009, MNRAS, 396, 291
Bruntt H., Frandsen S., Gilliland R. L., Christensen-Dalsgaard J., Petersen J. O., Guhathakurta P., Edmonds P. D., Bono G., 2001, A&A, 371, 614
Caldwell J. A. R., Cousins A. W. J., Ahlers C. C., van Wamelen P., Maritz E. J., 1993, South African Astron. Obser. Circ., 15, 1
Carretta E., Gratton R. G., Clementini G., Fusi Pecci F., 2000, ApJ, 533, 215
Carretta E., Bragaglia A., Gratton R., D'Orazi V., Lucatello S., 2009, A&A, 508, 695 (C09)
Carretta E., Bragaglia A., Gratton R. G., Recio-Blanco A., Lucatello S., D'Orazi V., Cassisi S., 2010, A&A, 516, 55
Casagrande L., Portinari L., Flynn C., 2006, MNRAS, 373, 13
Casagrande L., Ramirez I., Melendez J., Bessell M., Asplund M., 2010, A&A, 512, 54 (CRMBA)
Castanheira B. G., Breger M., Beck P. G., Elmasli A., Lenz P., Falcon R. E., 2008, Communications Asteroseismology, 157, 124
Catelan M., Grundahl F., Sweigart A. V., Valcarce A. A. R., Cortés C., 2009, ApJ, 695, L97
Chen X., Han Z., 2004, MNRAS, 355, 1182
Chen X., Han Z., 2008, in Deng L. C., Chan K.-L., eds, Proc. IAU Symp. 252, The Art of Modeling Stars in the 21st Century. Cambridge Univ. Press, Cambridge, p. 417
Coleman M. G., de Jong J. T. A., 2008, ApJ, 685, 933
Daszyńska-Daszkiewicz J., 2008, Commun. Asteroseismol., 152, 140
de Jong J. T. A., Rix H.-W., Martin N. F., Zucker D. B., Dolphin A. E., Bell E. F., Belokurov V., Evans N. W., 2008, AJ, 135, 1361
Dékány I., Kovács G., 2009, A&A, 507, 803
Di Criscienzo M., Ventura P., D'Antona F., Milone A., Piotto G., 2010, MNRAS, 408, 999
Di Criscienzo M. et al., 2011, MNRAS, 414, 3381
Dotter A., Chaboyer B., Jevremović D., Kostov V., Baron E., Ferguson J. W., 2008, ApJS, 178, 89
Dotter A. et al., 2010, ApJ, 708, 698 (D10)
Dupree A. K., Strader J., Smith G. H., 2011, ApJ, 728, 155
Fabrizio M. et al., 2011, PASP, 123, 384
Ferraro F. R. et al., 2006, ApJ, 647, L53
Frolov M. S., 1974, Sci. Inform. Astron. Council USSR Acad. Sci., 33, 29
Gerashchenko A. N., Kadla Z. I., Malakhova Y. N., 1999, Astron. Rep., 43, 20
Gilliland R. L., Bono G., Edmonds P. D., Caputo F., Cassisi S., Petro L. D., Saha A., Shara M. M., 1998, ApJ, 507, 818
Gratton R. G., Fusi Pecci F., Carretta E., Clementini G., Corsi C. E., Lattanzi M., 1997, ApJ, 491, 749
Gratton R. G., Bragaglia A., Carretta E., Clementini G., Desidera S., Grundahl F., Lucatello S., 2003a, A&A, 408, 529
Gratton R. G., Carretta E., Claudi R., Lucatello S., Barbieri M., 2003b, A&A, 404, 187
Gratton R. G., Carretta E., Bragaglia A., Lucatello S., D'Orazi V., 2010, A&A, 517, A81
Greco C. et al., 2009, ApJ, 701, 1323
Hanson R. B., 1979, MNRAS, 186, 875
Harris W. E., 1996, AJ, 112, 1487
Harris J., Zaritsky D., 2009, AJ, 138, 1243
Hartman J. D., Kaluzny J., Szentgyorgi A., Stanek K. Z., 2005, AJ, 129, 1596
Iben I., Jr, 1986, Mem. Soc. Astron. Ital., 57, 453
Jeon Y.-B., Kim S.-L., Lee H., Lee M. G., 2001, AJ, 121, 2769
Jeon Y.-B., Lee M. G., Kim S.-L., Lee H., 2003, AJ, 125, 3165
Jeon Y.-B., Lee M. G., Kim S.-L., Lee H., 2004a, AJ, 128, 287
Jeon Y.-B., Lee M. G., Kim S.-L., Lee H., 2004b, in Kurtz D. W., Pollard K. R., eds, ASP Conf. Ser. Vol. 310, Variable Stars in the Local Group. Astron. Soc. Pac., San Francisco, p. 166
Jeon Y.-B., Kim S.-L., Lee M. G., Lee H., Lee J. W., 2006, ApJ, 636, L129
Kaluzny J., Thompson I. B., 1999, A&A, 350, 469
Kaluzny J., Thompson I. B., 2003, AJ, 125, 2534
Kaluzny J., Thompson I. B., 2009, Acta Astron., 59, 273
Kaluzny J., Krzeminski W., Nalezyty M., 1997, A&AS, 125, 337
Kaluzny J., Olech A., Thompson I. B., Pych W., Krzeminski W., Schwarzenberg-Czerny A., 2004, A&A, 424, 1101
Kaluzny J., Thompson I. B., Krzeminski W., Schwarzenberg-Czerny A., 2006, MNRAS, 365, 548
Kaluzny J., Thompson I. B., Krzeminski W., Zloczewski K., 2010, Acta Astron., 60, 245
Kippenhahn R., Weigert A., 1967, Z. Astrophys., 65, 251
Knigge C., Leigh N., Sills A., 2009, Nat, 457, 288
Kopacki G., 2005, Acta Astron., 55, 85
Kopacki G., 2007, Acta Astron., 57, 49
Kravtsov V. V., Zheleznyak A. P., 2003, Inf. Bull. Var. Stars, 5452, 1
Leigh N., Sills A., Knigge C., 2011, MNRAS, 416, 1410
Lenz P., Pamyatnykh A. A., Zdrakov T., Breger M., 2010, A&A, 509, 90
Lombardi J. C., Jr, Rasio F. A., Shapiro S. L., 1995, ApJ, 445, L117
Lovisi L. et al., 2010, ApJ, 719, L121
Mackey A. D., Gilmore G. F., 2003, MNRAS, 345, 747
McNamara D. H., 1997, PASP, 109, 1221

McNamara D. H., Rose M. B., Brown P. J., Ketcheson D. I., Maxwell J. E., Smith K. M., Wooley R. C., 2004, in Kurtz D. W., Pollard K. R., eds, ASP Conf. Ser. Vol. 310, Variable Stars in the Local Group. Astron. Soc. Pac., San Francisco, p. 166
McNamara D. H., Clementini G., Marconi M., 2007, AJ, 133, 2752
Madore B. F., 1982, ApJ, 253, 575
Majaess D. J., Turner D. G., Lane D. J., Henden A., Kracji T., 2011, J. American Association Var. Star Obser., 39, 122
Marconi M., Ripepi V., Bernabei S., Ruoppo A., Monteiro M. J. P. F. G., Marques J. P., Palla F., Leccia S., 2010, Ap&SS, 328, 109
Marconi M., Bono G., Caputo F., Piersimoni A. M., Pietrinferni A., Stellingwerf R. F., 2011, ApJ, 735, 111
Marino A. F., Piotto G., Gratton R., Milone A. P., Zoccali M., Bedin L. R., Villanova S., Bellini A., 2010, in Charbonnel C., Tosi M., Primas F., Chiappini C., eds, Proc. IAU Symp. 268, Light Elements in the Universe. Cambridge Univ. Press, Cambridge, p. 183
Mateo M., Hurley-Keller D., Nemec J., 1998, AJ, 115, 1840
Mazur B., Kaluzny J., Krzeminski W., 1999, MNRAS, 306, 727
Milone A. P. et al., 2010, ApJ, 709, 1183
Moehler S., Dreizler S., Lanz T., Bono G., Sweigart A. V., Calamida A., Monelli M., Nonino M., 2007, A&A, 475, 5
Moretti M. I. et al., 2009, ApJ, 699, L125
Musella I. et al., 2009, ApJ, 695, L83
Nemec J., Mateo M., 1990, Confrontation Between Stellar Pulsation and Evolution, 11, 64
Nemec J. M., Park N., 1996, The Origins, Evolution, and Destinies of Binary Stars in Clusters, 90, 359
Nemec J. M., Linnell Nemec A. F., Lutz T. E., 1993, Blue Stragglers, 53, 145
Newsham G., Terndrup D. M., 2007, ApJ, 664, 332
Nikolaev S., Drake A. J., Keller S. C., Cook K. H., Dalal N., Griest K., Welch D. L., Kanbur S. M., 2004, ApJ, 601, 260
Olech A., Wozniak P. R., Alard C., Kaluzny J., Thompson I. B., 1999, MNRAS, 310, 759
Olech A., Dziembowski W. A., Pamyatnykh A. A., Kaluzny J., Schwarzen-Czerny A., Thompson I. B., 2005, MNRAS, 363, 40
Otulakowska M., Olech A., Pych W., Pamyatnykh A. A., Zdravkov T., Rucinski S. M., 2011, Acta Astron., 61, 161
Park N.-K., Nemec J. M., 2000, AJ, 119, 1803
Pasquini L., Mauas P., Käufl H. U., Cacciari C., 2011, A&A, 531, 35
Petersen J. O., Christensen-Dalsgaard J., 1999, A&A, 352, 547 (PCD99)
Petersen J. O., Freyhammer L. M., 2002, in Aerts C., Bedding T. R., Christensen-Dalsgaard J., eds, ASP Conf. Ser. Vol. 259, Radial and Nonradial Pulsations as Probes of Stellar Physics. Astron. Soc. Pac., San Francisco, p. 136 (PF02)
Piersimoni A. M., Bono G., Ripepi V., 2002, AJ, 124, 1528
Pietrzynski G., Gorski M., Gieren W., Ivanov V. D., Bresolin F., Kudritzki R.-P., 2009, AJ, 138, 459
Piotto G. et al., 2005, ApJ, 621, 777
Piotto G. et al., 2007, ApJ, 661, L53
Poleski R. et al., 2010, Acta Astron., 60, 1
Poretti E., 1999, A&A, 343, 385
Poretti E. et al., 2008, ApJ, 685, 947 (P08)
Pych W., Kaluzny J., Krzeminski W., Schwarzenberg-Czerny A., Thompson I. B., 2001, A&A, 367, 148
Raghavan D. et al., 2010, ApJS, 190, 1
Richer H. B. et al., 1997, ApJ, 484, 741
Rizzi L., Held E. V., Saviane I., Tully R. B., Gullieuszik M., 2007, MNRAS, 380, 1255
Rodríguez E., Breger M., 2001, A&A, 366, 178
Rodríguez E., López-González M. J., 2000, A&A, 359, 597
Rodríguez E. et al., 2007, A&A, 471, 255
Rubenstein E. P., Bailyn C. D., 1993, Blue Stragglers, 53, 173
Safonova M., Stalin C. S., 2011, preprint (arXiv:1105.4363)
Salaris M., Chieffi A., Straniero O., 1993, ApJ, 414, 580
Salinas R., Catelan M., Smith H. A., Pritzl B. J., 2007, Inf. Bull. Var. Stars, 5744, 1
Santolamazza P., Marconi M., Bono G., Caputo F., Cassisi S., Gilliland R. L., 2001, ApJ, 554, 1124 (S01)
Sarajedini A. et al., 2007, AJ, 133, 1658
Sarna M. J., De Greve J.-P., 1996, QJRAS, 37, 11
Schlegel D. J., Finkbeiner D. P., Davis M., 1998, ApJ, 500, 525
Sirianni M. et al., 2005, PASP, 117, 1049
Smecker-Hane T. A., Stetson P. B., Hesser J. E., 1994, AJ, 108, 507
Sollima A., Cacciari C., Bellazzini M., Colucci S., 2010, MNRAS, 406, 329
Soszynski I. et al., 2003, Acta Astron., 53, 93
Suárez J. C., Garrido R., Goupil M. J., 2006, A&A, 447, 649
Templeton M. R., Guzik J. A., McNamara B. J., 1998, BAAS, 30, 1339
Templeton M., Basu S., Demarque P., 2002, ApJ, 576, 963
Testa V., Chieffi A., Limongi M., Andreuzzi G., Marconi G., 2004, A&A, 421, 603
Thompson I. B., Kaluzny J., Pych W., Krzeminski W., 1999, AJ, 118, 462
van den Bergh S., 1968, J. R. Astron. Soc. Can., 62, 145
van Leeuwen F., 2007, A&A, 474, 653
VandenBerg D. A., Bergbusch P. A., Dowler P. D., 2006, ApJS, 162, 375
Villanova S., Piotto G., Gratton R. G., 2009, A&A, 499, 755
Walker A. R., 1994, AJ, 108, 555
Weldrake D. T. F., Sackett P. D., Bridges T. J., 2007, AJ, 133, 1447

APPENDIX A: SX PHE SELECTION

Here we list details regarding the sources of the SX Phe pulsational and photometric properties given in Table 3.

NGC 104 (47 Tuc): properties of V1 are from Gilliland et al. (1998) and properties of the remaining SX Phe are taken from Bruntt et al. (2001). Since the latter study failed to detect variability in V14, we have excluded it from our catalogue.

NGC 288: the colours reported by Kaluzny, Krzeminski & Nalezyty (1997) are based on only one image in the *B* filter and therefore are likely somewhat uncertain.

NGC 1261: SX Phe discovered by Salinas et al. (2007)

NGC 2419: SX Phe discovered and characterized by Di Criscienzo et al. (2010). Based on its period and magnitude, V83 is not a radial pulsator.

NGC 4590 (M68): both SX Phe discovered by Walker (1994).

NGC 5024 (M53): Jeon et al. (2003) find that SXP2 (= V74) is a non-radial pulsator and SXP8 is multiperiodic. Dékány & Kovács (2009) discovered additional likely SX Phe in M53, but they could obtain a standard magnitude and colour for only one (V77), which is not included in Arellano Ferro et al. (2011) or Safonova & Stalin (2011). Six SX Phe observed by Jeon et al. (2003) were also detected by both Arellano Ferro et al. (2011) and Safonova & Stalin (2011): SXP1-3 and SXP5-7 (= V73, V74, V87, V89, V75, V76, respectively), and in these cases we use the properties given by Arellano Ferro et al. (2011) since their time series investigation contains both a greater number of observations and a longer time baseline. By matching the coordinates of the newly discovered SX Phe from these two studies, we found that there are seven SX Phe in common: V96, V97, V99, V101, V102, V103, V105 (= SX2, SX3, SX9, SX11, SX14, SX19, SX22, respectively), and the properties of these stars are taken from Arellano Ferro et al. (2011) as well.

NGC 5053: Arellano Ferro, Giridhar & Bramich (2010) suggest that BS5 and BS25 are first overtone pulsators and confirm the double radial mode nature of NC13.

NGC 5139 (ω Cen): pulsation modes of SX Phe from Olech et al. (2005) were identified based on the analysis in their Appendix A and double radial mode pulsators based on their Fig. 7. They report that the photometry of OGLEGC2 (= V198), NV299 and NV321 is uncertain and suspect OGLEGC4 (= V200) of being a foreground star. ($V - I$) colours given for SX Phe in the Olech et al. (2005) study

are from Kaluzny et al. (1997) and were decreased by 0.056 mag following Kaluzny et al. (2004). These $(V - I)$ colours are colours at maximum light rather than mean values. The remaining SX Phe not identified in these studies (V7, V22, V23, V92 and V131) were reported by Weldrake et al. (2007), whose magnitudes and colours are based on three images in each filter and hence may be somewhat uncertain (see Section 3.2). In addition, the $(V - I)$ colour of OGLEGC39 (= V232) is from Weldrake et al. (2007).

NGC 5272 (M3): Nemec & Mateo (1990) classified the star marked 'Anon' as a likely first overtone pulsator. Nemec & Park (1996) report periods for SE174, NW449 and NW858, although their colours are likely somewhat uncertain (see Section 3.2). The remaining variables are from from Hartman et al. (2005). For NV291, updated properties from Benkő, Bakos & Nuspl (2006) are given.

NGC 5466: mode identification is from Jeon et al. (2004a).

NGC 5904 (M5): properties of V1, V3 and V4 are from Kaluzny & Thompson (1999), and V160 is from Olech et al. (1999).

NGC 6205 (M 13): properties are from Kopacki (2005), who identify v46 as a probable multiple radial mode pulsator.

NGC 6341 (M92): properties of SX Phe are from Kopacki (2007), who suspect that V34 is a double radial mode pulsator if their detected period is affected by aliasing.

NGC 6362: variables V46-48 have uncertain periods (Mazur, Kaluzny & Krzeminski 1999), and the colours of all four SX Phe reported in that study are based on only two frames and hence may be uncertain.

NGC 6366: Arellano Ferro et al. (2008) identified the pulsation modes of V6 as fundamental and an additional non-radial mode.

NGC 6397: the four candidate SX Phe from Rubenstein & Bailyn (1993) have uncertain periods. The properties of the remaining SX Phe (V10, V11, V15, V21, V23) are from Kaluzny & Thompson (2003) and Kaluzny et al. (2006).

NGC 6715 (M54): SX Phe properties are taken from Sollima et al. (2010), who suspect at least one of these stars of being non-members or members of the Sagittarius DSph based on their periods and magnitudes.

NGC 6752: V7 and V12 are analysed by Kaluzny & Thompson (2009) and properties of V13 are from Thompson et al. (1999).

NGC 6809 (M55): periods and magnitudes were taken from Kaluzny et al. (2010). Double radial-mode and non-radial pulsators were identified by Pych et al. (2001) based on their period ratios, but see the footnote in section 5 of P08, who suspect that V21 is a rotational variable.

NGC 6838: H1 is a first overtone pulsator according to Nemec & Mateo (1990). However, if this star is also D6 of Jeon et al. (2004b) then it is a double radial mode pulsator. V13 of Park & Nemec (2000) has an uncertain period, and we have excluded V9 and V22, which they identify as candidate variables but were not able to determine a period for. QU Sge is a component of a binary system analysed by Jeon et al. (2006).

NGC 6981: based on the study of Bramich et al. (2011), V55 and V56 are likely pulsating in a different mode than the double radial mode pulsator V54.

NGC 7078 (M15): ZK62 and ZK68 were identified by Kravtsov & Zheleznyak (2003) via *R*-band time series, and SXP1 was identified by Jeon et al. (2001).

SUPPORTING INFORMATION

Additional Supporting Information may be found in the online version of this article:

Table 3. SX Phe in Galactic globular clusters.

Please note: Wiley-Blackwell are not responsible for the content or functionality of any supporting materials supplied by the authors. Any queries (other than missing material) should be directed to the corresponding author for the article.

This paper has been typeset from a TEX/LATEX file prepared by the author.